Hindawi
International Journal of Antennas and Propagation
Volume 2019, Article ID 5076139, 12 pages
https://doi.org/10.1155/2019/5076139

Research Article

RFID Double-Loop Tags with Novel Meandering Lines Design for Health Monitoring Application

Ibtissame Bouhassoune,[1] **Rachid Saadane**,[2] **and Khalid Minaoui**[1]

[1]*LRIT Laboratory, Faculty of Science, Mohammed V University, Rabat, Morocco*
[2]*SIRC/LaGeS-EHTP, EHTP Km 7 Route El Jadida, Oasis, Morocco*

Correspondence should be addressed to Ibtissame Bouhassoune; i.bouhassoune@gmail.com

Received 24 March 2019; Revised 16 July 2019; Accepted 25 August 2019; Published 1 October 2019

Guest Editor: Sandra Costanzo

In this paper, we propose a design of two compact and miniaturized RFID epidermal tags in the UHF band for health monitoring applications. The two conceptions of meandered double-loop antennas with *T*-match configuration, namely, a double-loop antenna with meandered line in the horizontal direction and a double-loop antenna with meandered lines in two directions, are placed at very close distance from the human body. The proposed tags are composed of bio-silicone substrate, to protect the human skin from the electromagnetic waves, and a copper conductor loaded by *T*-match configuration, to suit the complex impedance of the antenna to that of the chip. We have performed numerical simulations of these conceptions of two tags using the HFSS and CST solvers. Our results show two optimal sizes with a high communication performance, good matching features, and a large read range. We placed afterwards these two optimized tags in an elliptical environment to test their flexibility and examine their performance on different parts of the human body.

1. Introduction

One of the most striking evolutions of radiofrequency identification (RFID) is manifested in the epidermal RFID family for human health monitoring applications and indoor/outdoor tracking systems. This new RFID technology plays two roles, the first one is to identify different objects, and the second one is to sense physiological parameters of the human body (temperature, pressure, heartbeat, etc.). Therefore, the healthcare system can be highly developed and monitored in the long term.

The RFID system is composed of remote tags and interrogators or readers devices. The former has the potentiality to properly collect the energy from the readers and store the data in the microchip, while the latter transmit and receive the radio waves to communicate with tags [1] (see Figure 1).

The RFID tags can be passive without an internal power source, collecting energy from the interrogator, or semi-passive when a battery is used only to power and run the chip or other electronic components, and can be active when the tag has its own local alimentation system, which directly feeds a tag chip and the transmitting radio channel [2].

The epidermal RFID tags are placed in direct touch with human skin, and fabricated with a very thin, flexible, and biocompatible material, acting as an insulator between the conductor/electronic components and the skin. However, the cohabitation of passive tag elements with the human skin represents a complex challenge due to high losses in human tissues which strongly affect the general properties of the antenna. The electromagnetic waves emitted by the reader are either reflected or absorbed by the human tissue, and therefore, the performance of the wireless communication diminishes [3]. Most of the scientific researchers presented until now have been oriented to integrate the antenna with the lossy body, while maintaining the best characteristics of the antenna.

The epidermal RFID technology has been focused first on the near field, at 13.56 MHz (HF RFID), thanks to its insensitivity to the presence of living tissues and its

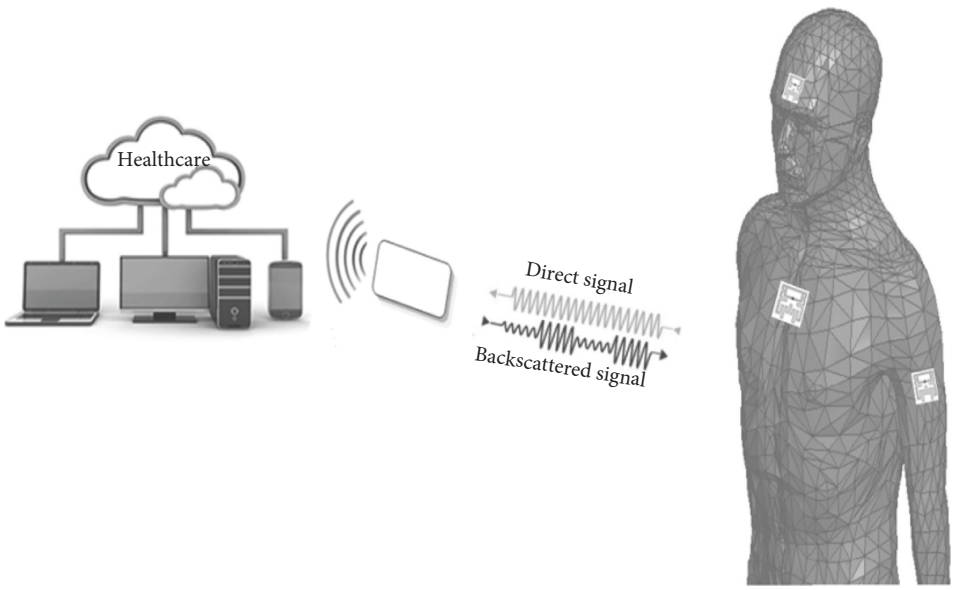

Figure 1: Concept of the RFID epidermal backscattering principle.

simplified design which consists of multiturn strip antennas attached to the chip. The basic function of this type of system is the inductive coupling which allows the readability by the reader only at small distances from the skin [4]. Thus, the feasibility of the HF standard in the wide environment, like supervising the body health in the hospital or at home, becomes limited.

Some successful works in the healthcare technology have extended the epidermal RFID systems to the UHF band (840–960 MHz). However, they are highly influenced by high dielectric objects as the human skin, but in principle, they can provide a long activation distance range. This potentiality opens additional possible sensing applications, where the patients can be monitored all the time by using the remote reader placed within environments like smart homes and hospitals [3]. Thus, the UHF RFID band is an attractive candidate than the HF band for this kind of applications, and it is therefore the subject of our study.

Various developments in the UHF RFID technology for human monitoring applications presented so far are interested to the innovative biosensor/tag with miniaturized size, reduced cost for wearable applications, like a famous slotted patch tag combined with a motion sensor, or fabricated with textile materials, which permits to decouple the antenna from the lossy human tissues [5, 6], and also double *T*-slotted patch designed for wristbands applications [7].

However, much less attention has been paid to the investigation and design of RFID antennas that are placed in direct contact with human skin and operated in the UHF band.

Recently considerable works on dual-loop tag placed in different body regions (stern, abdomen, limb, and head) [8] show the effects of each body regions of different volunteers on the antenna-matching features and realized gain. In ref. [9], the authors proposed a miniaturized dual-loop tag for temperature monitoring applications, with *T*-match configuration and tuning mechanism, to adapt its response to the specific placement over the body. This tag is used like a temporary epidermal RFID thermometer, and its read range can be significantly enhanced by adding a microbattery [9].

In this paper, we address in detail the conception and optimization of the design and communication performances of the RFID double-loop epidermal tag for the UHF band, with a goal to reach smaller size, more flexibility, and better radiation performance.

Our paper is organized as follows. In Section 2, we present the energetic constraints of the epidermal RFID systems. Sections 3 includes (1) the design of the first proposed epidermal tag, (2) its performance characteristics and the comparison between the results obtained from the HFSS and those examined in the CST solver, in order to confirm the simulated performances of our novel proposed tag, (3) the effects of the elliptical reference model of human torso on the first proposed tag, and (4) the investigation of the placement of the proposed tag on some human body parts. Finally, (5) the miniaturization of the first proposed tag and its communication features are also discussed in this section, followed by a conclusion in Section 4.

2. Electromagnetic Equations for UHF RFID Technology

It is widely known that the passive and semi-active tags collect the energy from the reader. To setup the wireless communication between the reader and tag, first, the reader has to send an EM wave that bears the necessary energy to activate the tag. In this step, the microchip has an input impedance $Z_{\text{chip}} = R_{\text{chip}} + jX_{\text{chip}}$, where R_c is the microchip resistance and X_{chip} is the capacitive reactance.

The impedance mismatch between the antenna $Z_{\text{ANT}} = R_{\text{ANT}} + jX_{\text{ANT}}$ and the tag is described by the power transfer coefficient:

$$\tau = \frac{4R_{\text{chip}}R_{\text{ANT}}}{\left|Z_{\text{chip}} + Z_{\text{ANT}}\right|^2} \leq 1. \quad (1)$$

This accounts for the impedance mismatch between the antenna and microchip and is maximum in the case, where the microchip can use the entire power available at the tag antenna, and conjugate impedance condition is achieved, $Z_{\text{chip}} = Z^*_{\text{ANT}}$.

In the next step of the wireless communication, the activated tag receives the signal from the reader, and finally sends back the data stored in the microchip memory through a backscattered modulation of the EM wave transmitted by the reader.

Within the hypothesis of free-space interactions, the direct link power represents a power balance between the power transmitted from the reader towards the tag, and the power needed to activate the microchip, whereas the backward link power quantifies the capability of the reader to detect the tag response. These powers are given by the Friis formula and the radar equations [2]:

$$P_{R\longrightarrow T} = \left(\frac{\lambda_0}{4\pi d}\right)^2 P_{\text{in}} \cdot G_R(\theta,\phi) \cdot G_\tau(\theta,\phi) \cdot \eta(\theta,\phi),$$

$$P_{R\longleftarrow T} = \left(\frac{\lambda_0}{4\pi d}\right)^4 P_{\text{in}} G_R^2(\theta,\phi) \cdot G_T^2(\theta,\phi)\eta^2(\theta,\phi) \cdot \tau \frac{4R_A^2}{\left|Z_c + Z_A\right|^2}, \quad (2)$$

where $G_\tau(\phi,\theta) = G_T(\phi,\theta).\tau$ is the realized gain of the tag, P_{in} is the power emitted by the reader, G_R is the reader antenna gain, η and d are the polarization factor and the read range distance between the reader and tag antenna, respectively, and λ_0 is the free-space wavelength.

The realized gain $G_\tau(\phi,\theta) = G_T(\phi,\theta) \cdot \tau$ is given by the radiation gain G_T of the tag antenna reduced by the power transfer coefficient τ between the tag antenna and the microchip.

$G_\tau(\phi,\theta)$ can be expressed in terms of the minimum input power $P_{\text{in}}^{\text{to}}$, emitted by the reader, to activate the microchip P_{chip}:

$$G_\tau(\theta,\phi) = \left(\frac{4\pi d}{\lambda_0}\right)^2 \frac{P_{\text{chip}}}{G_R(\theta,\phi) \cdot \eta(\theta,\phi) \cdot P_{\text{in}}^{\text{to}}(\theta,\phi)}. \quad (3)$$

The maximum distance $d_{\max}$, at which a tag is detected by the reader, represents an important parameter of the whole communication performance and can be derived from Friis equations.

$$d_{\max}(\theta,\phi) = \frac{C}{4\pi f}\sqrt{\frac{\text{EIRP}_R}{P_{\text{chip}}}\tau G_T(\theta,\phi)}, \quad (4)$$

where $\text{EIRP}_R = G_R \cdot P_{\text{in}}$ is the equivalent isotropic radiated power emitted by the reader and fixed according to the regulations of different countries. In particular, within the 865.6–867.6 MHz Europe RFID band, the EIRP_R is fixed at 3.2 W EIRP, and within 902–928 MHz USA RFID band, the EIRP_R is fixed at 4 W [3].

The presence of the lossy body with its high permittivity and conductivity will be useful for antenna miniaturization but induces a great dissipation of the electromagnetic power, which leads to degradation of the radiation gain. Therefore, a much shorter reading range is expected for skin-mounted RFID.

3. Antennas Conception

Our proposed epidermal tag designs are based on the conception presented in [8]. However, our suggested tag layouts have a small size; contain a flexible bio-silicone substrate in the ground surface, and are fully covered by adhesive copper.

The two proposed tags form double-loop antennas with meandered strips. The first one is composed of an external, meandered radiating loop, which is curved in the horizontal direction to eliminate the nonuseful strips (Figure 2). The second one is composed of an external, fully meandered loop and is schematized in Figure 3. The meandered strip antennas of our two tags are connected to the microchip by the *T*-match technique to match the complex impedances of the chip and antenna [10].

The conceptions of two proposed tags were discussed and analyzed according to our electromagnetic simulations, where the geometrical parameters were performed by EM Simulators HFSS and CST software [11, 12].

Our modulations are based on the assumption that tags are placed on an estimated model of the layered anatomical phantom of human torso at 870 MHz. This model consists of stratified parallelepiped boxes with defined properties such as thickness, dielectric constant, and conductivity. We took these parameters from the database given in ref. [13] (Figure 4).

3.1. Epidermal Tag with Meandered Lines in the Horizontal Direction Design. The first tag layout contains a bio-silicone substrate (permittivity = 2.5, $\sigma = 0.005$·S/m, thickness 0.6 mm) that has the same shape of the antenna, and copper tapes forming two loops attached by the *T*-match structure, which is designed to connect the antenna to the microchip Zchip = 16−j148 Ω and Pchip = −15 dBm). The *T*-match technique also furnishes a degree of liberty to tune the desired conjugate impedance match between the antenna and the chip. The presence of the horizontal meandered line in the external loop permits an increase of the current flow, meaning that the electrical length of the antenna increases, and hence the antenna's radiation performance presents a good immunity of the tag to the human body. As it is known, this later represents a very lossy object that strongly degrades the radiation pattern and efficiency of the antenna. The design and geometrical parameters of the proposed antenna are presented, respectively, in Figure 2 and Table 1.

3.2. Matching Features and Radiation Performances of the First Proposed Tag. The return loss of this antenna was calculated based on the power reflection coefficient which considers the impedance of the microchip Z_c and the antenna's conjugate impedance Z^*_{ANT} is as shown in the following equation [14]:

$$\left|S^2\right| = \left|\frac{Z_{\text{chip}} - Z_A^*}{Z_c - Z_A}\right|^2. \quad (5)$$

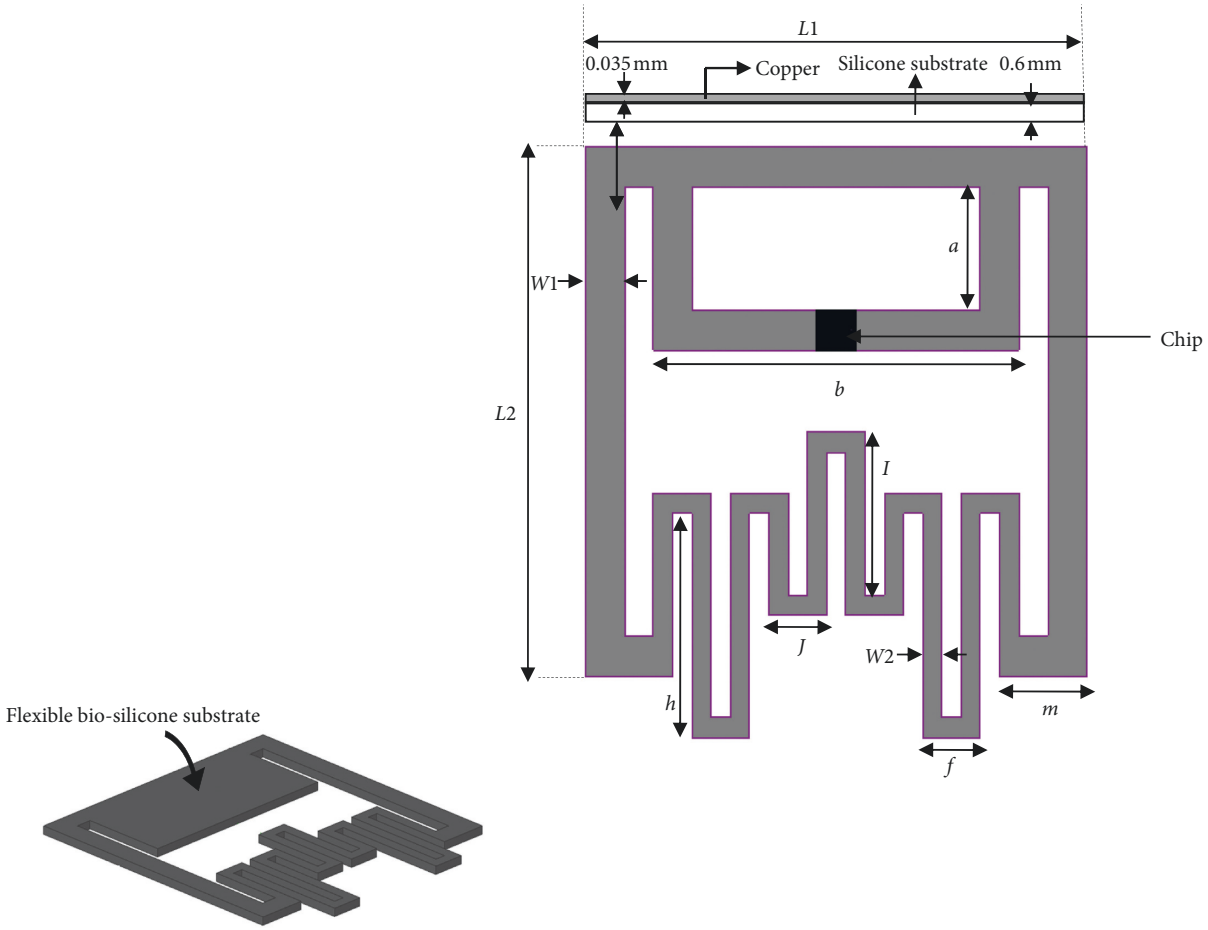

Figure 2: Geometrical design of dual loop tag with meandered line in the horizontal direction.

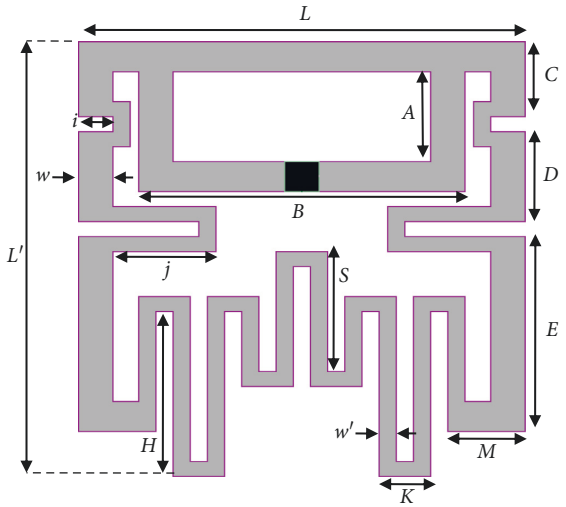

Figure 3: Geometrical layout of epidermal dual-loop tag with meandered lines in two directions.

Figure 5(a) shows the $S11$ plot against frequency of the first proposed tag antenna when it is placed on the human torso phantom.

The maximum simulated $S11$ of this tag has a value of −56.26 dB at the resonance frequency of 920 MHz.

The input impedance of the first proposed antenna is plotted in Figure 5(b). We can notice from the graph that the input impedance of the antenna, at the resonance frequency 920 MHz, is $Z_{\text{in}} = 16.5 + j148\,\Omega$. However, the input resistance of the antenna on the human torso is little higher

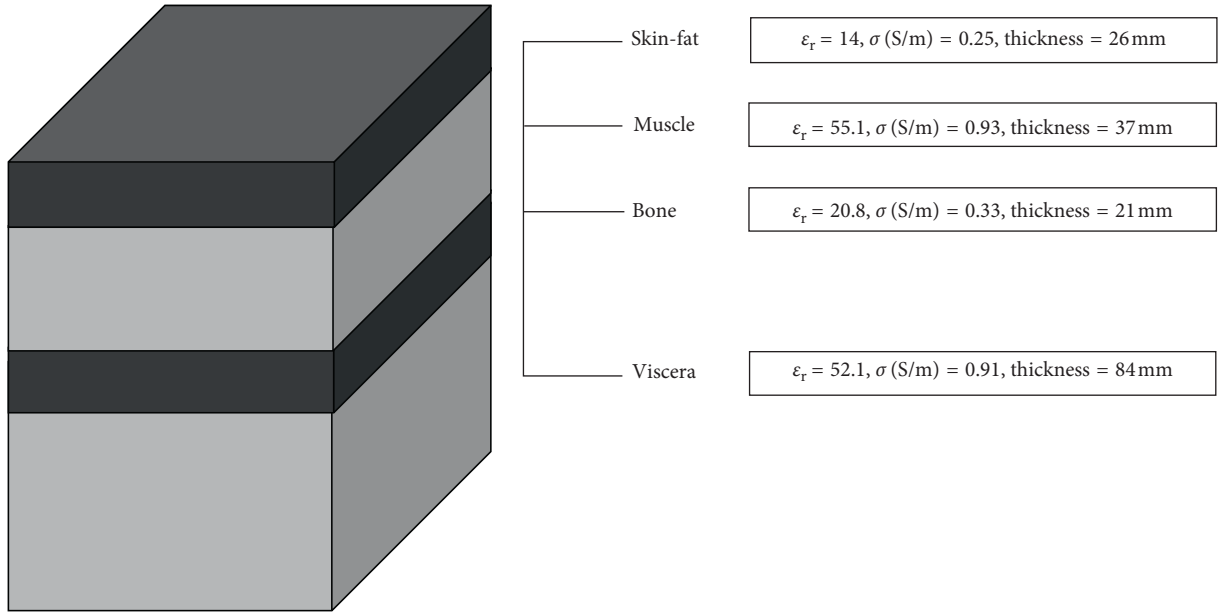

Figure 4: Geometrical and electrical parameters of the layered anatomical phantom of human torso at 870 MHz.

Table 1: Optimal dimensions of the first proposed epidermal RFID antenna.

Geometrical parameters	Dimensions (mm)
$L1 = L2$	26
A	6
B	19
M	4.5
F	3
I	9
J	3
H	12
$W1$	2
$W2$	1

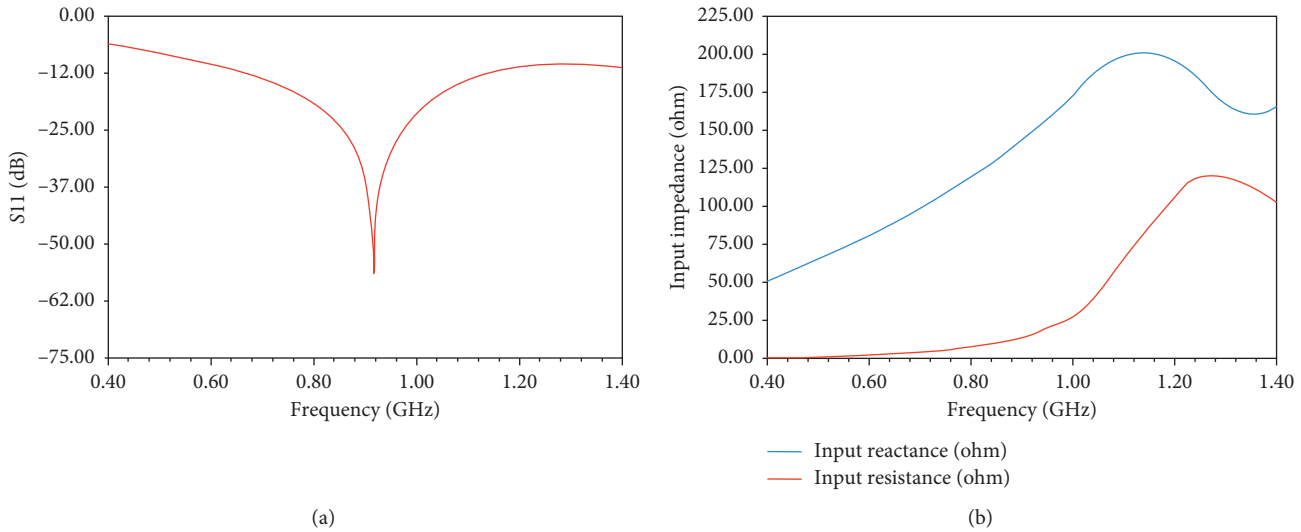

Figure 5: Simulated reflection coefficient S_{11} (a) and antenna input impedance (b) of the first proposed epidermal tag attached to the human torso model.

(about 16.50 Ω) than the resistance of the tag chip (16 Ω). The antenna input reactance is well conjugated to the tag chip reactance ($-j148\,\Omega$) around 920 MHz.

The realized gain simulation versus frequency, depicted in Figure 6, is obtained using a soft HFSS to simulate the performance of antenna radiation. In this case, the microchip was modeled by introducing the lumped port that simulates the behavior of the chip (with its complex impedance feed) [15]. The maximum value of the realized gain is −10.54 dBi, obtained around 960 MHz.

The 2 D radiation pattern of the first tag antenna attached to the planar torso model is presented in Figure 7. One can notice, from this figure, that the antenna represents a good omnidirectional radiation patterns in the two planes. Since the human tissues obviously absorb some of the received electromagnetic radiation, in our case, the peak gain is also reduced due to the effects of the human torso (−9.59 dBi around 960 MHz). In Figure 8, the simulated data refer to the estimated read range between tag and reader. When our first proposed tag was stacked onto the human body, the maximum read distance is almost 2.34 m in the case of the reader with circular polarization ($\boldsymbol{\eta_p} = 0.5$), and it becomes above 4.68 m in the case of the reader with linear polarization ($\boldsymbol{\eta_p} = 1$).

To verify the HFSS simulation results of our antenna characteristics, such as the S_{11} and the realized gain, we have used, for a comparison, another simulator (CST simulator) to design and simulate our first proposed antenna. The curves of S_{11} and the realized gain obtained from the CST and HFSS solvers are shown, respectively, in Figures 9(a) and 9(b). Nearly similar matching features and radiation performance are obtained from the two solvers. The slight differences between the results of the two simulators can be attributed to the difference between the numerical codes of each simulator and the mesh used during the simulation.

3.3. Deformation Effects on the First Proposed Tag Antenna. In order to take into account the effect of deformation, that also may happen to different parts of the human skin, we placed our epidermal tag on a layered elliptical model, of the human torso, taken from the database of ref. [16] (see Figure 10). This model helps us to see what happens to the antenna performance, compared to the previous planar model, when the effect of the curved meandered loop surface is taken into consideration.

Figure 11 shows *S*11 of our antenna by assuming two models of the human torso as described above: the planar (no simulated bending) and the elliptical layered model. We found that *S*11 in the antenna-bending format (elliptical model) at the resonance frequency ($S_{11} = -46$ dB) is slightly different from the one in the planar model ($S_{11} = -56$ dB). This effect can also be clearly seen in Figure 12 where a slight difference, in the input resistance between the elliptical and the planar form of the antenna, is noticed around the resonance frequency of 920 MHz.

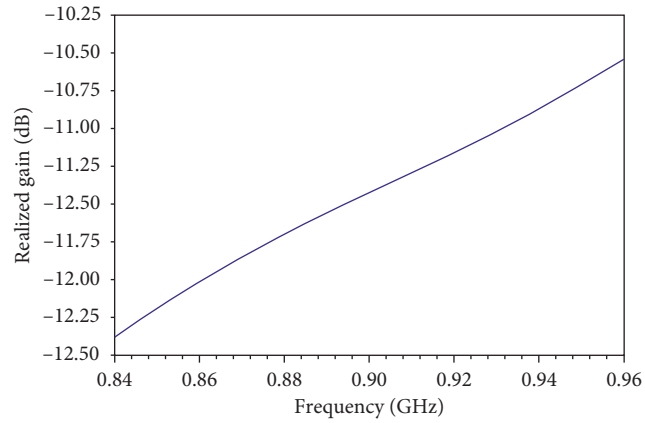

Figure 6: Simulated realized gain versus frequency of the first proposed epidermal tag over the human body reference model.

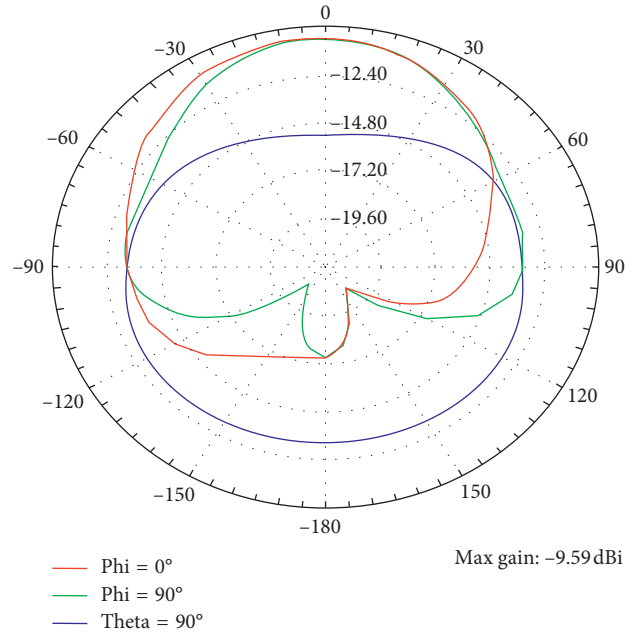

Figure 7: Radiation pattern (gain-total) in 2 D of the proposed epidermal tag over the human body reference model.

3.4. Simulated Performances of the First Proposed Antenna against Human Body Parts. In the following, we examine the properties of the first tag when it is bound to different parts of the body. Table 2 shows reference tissue thicknesses of some human body parts in the undistorted planar model. Figures 13(a) and 13(b) show, respectively, the simulated *S*11 and gain of our epidermal tag placed on four parts of the human body. The latter represents two regions according to the thickness of the fat tissue, i.e., the first region is characterized by small thicknesses (wrist and chest) while the second one has large thicknesses (abdomen and limb). We remark a decrease of *S*11 in the case when the tag is placed on the chest and wrist part. Moreover, we note that for the abdomen and the limb, the gain reaches higher values because of the high contents of fat tissue in the abdomen and limb compared to the chest and the wrist.

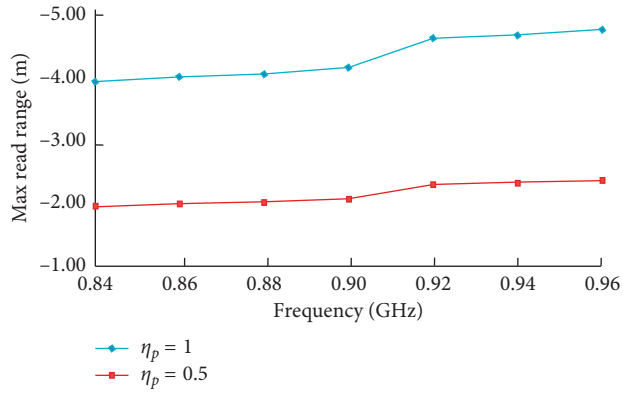

Figure 8: Read range of the epidermal RFID double-loop tag with meandered line in the horizontal direction.

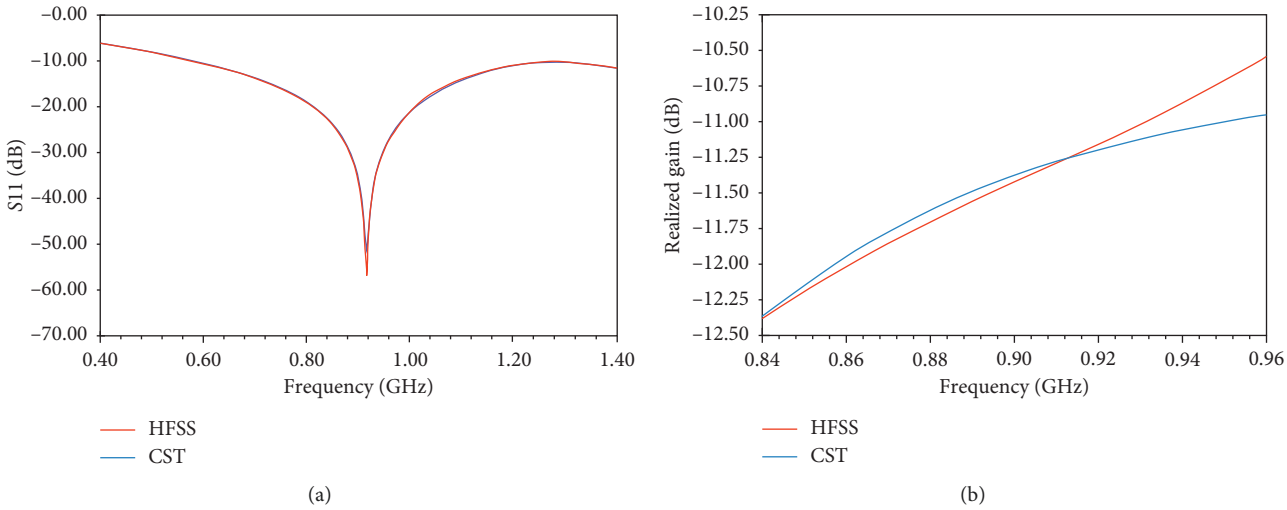

Figure 9: Comparison of the S11 results (a) and realized gain (b) of the first proposed antenna between the two simulators HFSS and CST.

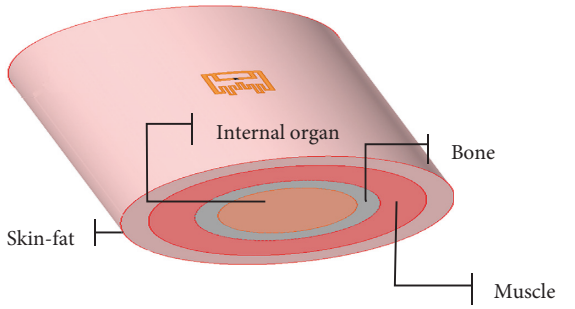

Figure 10: The first proposed tag placed on the layered elliptical model of the human torso: skin-fat axes, $335 \times 168\,mm^2$; muscle ellipse axes, $310 \times 142\,mm^2$; bone ellipse axes, $284 \times 105\,mm^2$; internal organ, $272 \times 84\,mm^2$ at 870 MHz.

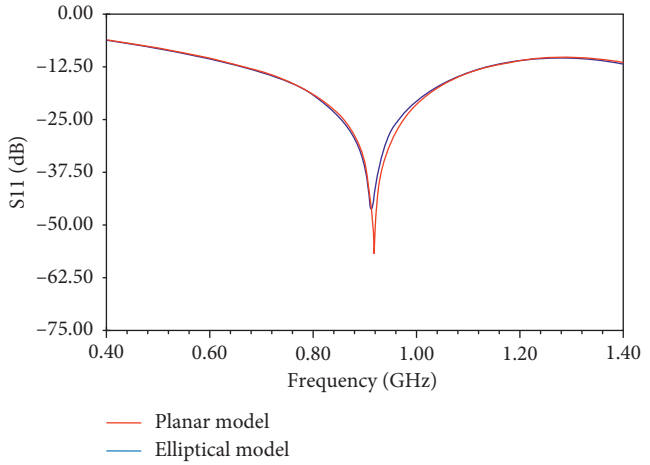

Figure 11: Simulated S11 of the first proposed tag on the layered elliptical model and planar model.

3.5. Epidermal Tag with Meandered Lines in the Two Directions Design. Figure 3 shows our second proposed tag whose shape is derived from the first tag addressed above, after miniaturization of the external loop, by adding meandered lines, not only in the horizontal direction but also in the vertical direction. The internal loop was connected to the chip by a T-match impedance transformer, and the chip has an input impedance $Z_{in} = 23.3 - j145\,\Omega$ and a power sensitivity (Pc = −4.5 dbmw). This tag is stuck over the human skin by a

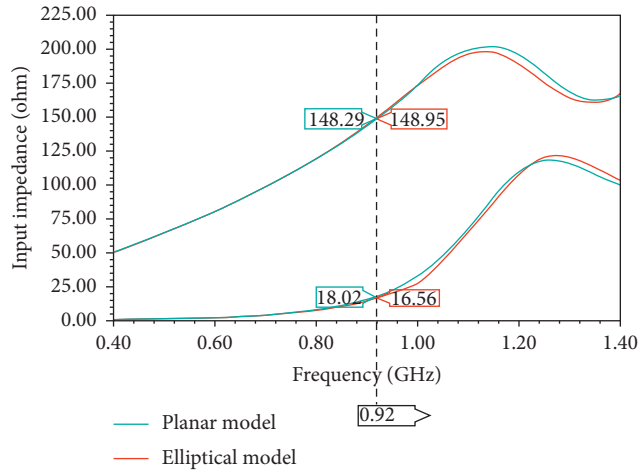

Figure 12: Simulated input resistance and reactance of the first proposed tag antenna on the layered elliptical model and planar model.

Table 2: Thicknesses of different tissues for some human body parts in the planar model.

Tissue thickness (mm)	Abdomen	Limb	Chest	Wrist
Skin	2	2.5	3	2
Fat	10	8	3	2
Muscle	20	25	20	24
Bone			11	10

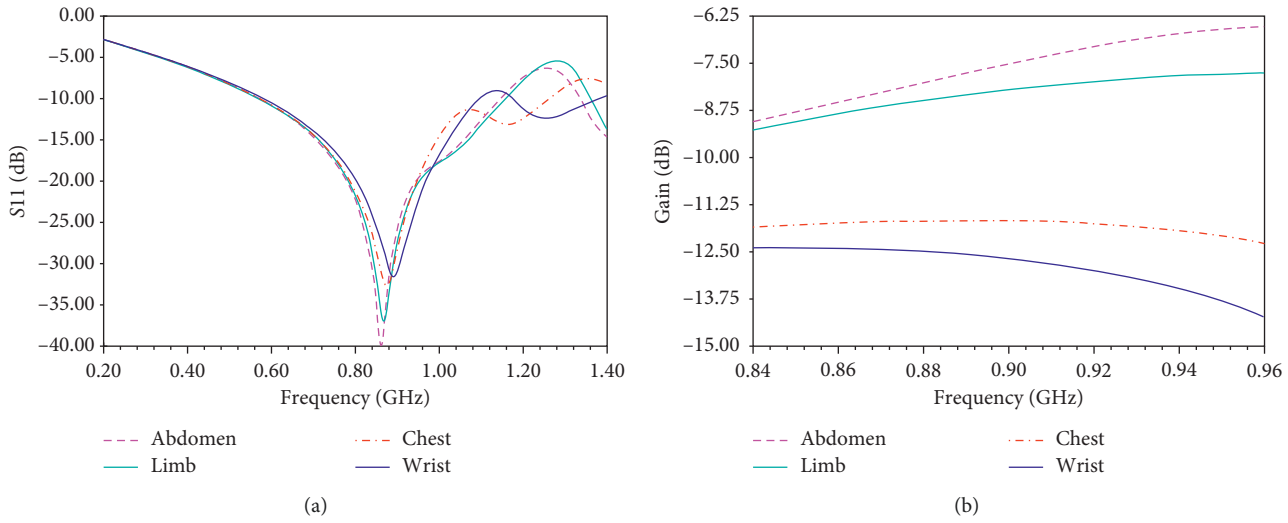

Figure 13: Simulated $S11$ (a) and gain (b) of the first epidermal tag placed on some human body parts (abdomen, limb, chest, and wrist).

sub-millimeter bio-silicone rectangular layer ($L = 26$ mm, L' = 29 mm and thickness = 0.6 mm) and is designed by numerical simulations using the finite element method implemented in the HFSS solver. As in the previous simulation, we consider the same human body reference model. The antenna geometrical parameters are tabulated in Table 3.

Figure 14(a) shows the reflection coefficient S_{11} of the epidermal double-loop tag with meandered lines in two directions. The peak $S11$ is now −46.35 dB at resonance frequency 900 Mhz. Figure 14(b) shows the input impedance plots of the second proposed antenna. The simulated resistance for the antenna in the UHF RFID frequency range maintains a value close to 23.3 ohms. The input reactance of the second antenna, as shown in Figure 14(b), maintains a positive value with a linear variation with frequency that equivalently cancels the effect of the capacitance of the chip. Therefore, the input impedance value of the antenna is almost matched with that of the tag chip around 900 MHz.

We note, from Figure 15, that the maximum realized gain of the second proposed tag is −10.80 dBi, at around 960 MHz. This value is lower than that of our previous tag, but it still maintains a good realized gain compared to other epidermal tags presented in the literature [8].

Figure 16 presents the 2 D radiation pattern of our second antenna which has similar omnidirectional radiation patterns as the first one, and as described above, the human

Table 3: Dimensions of the second proposed epidermal antenna.

Parameter	Dimension (mm)
L	26
L'	29
A	6
B	19
C	5
D	6
E	13
M	4.5
K	3
S	8
H	11
I	2
J	6
W	2
W'	1

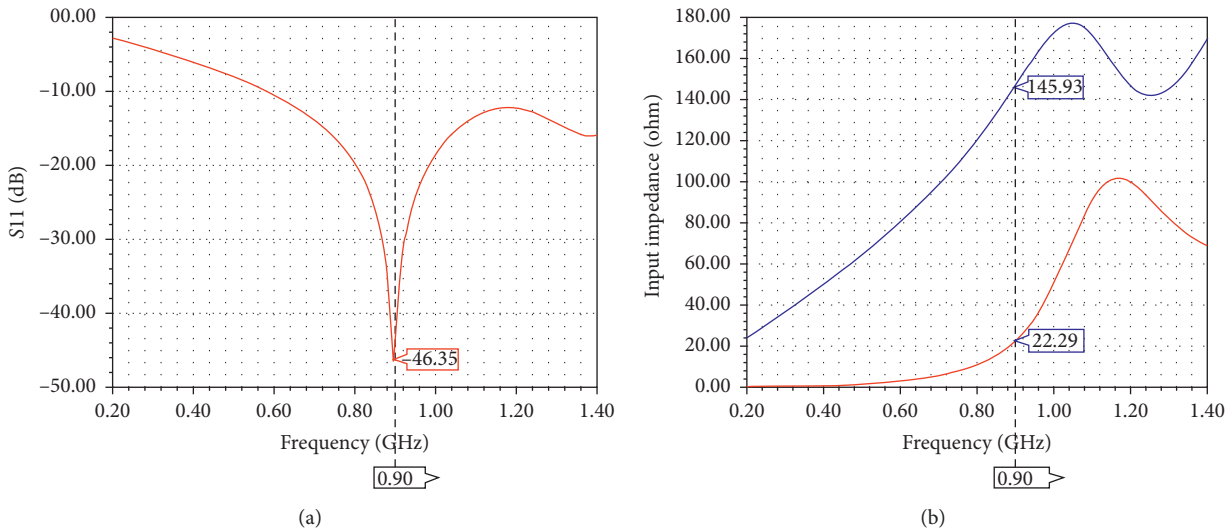

Figure 14: Simulated $S11$ (a) and antenna input impedance (b) of the epidermal double-loop tag with meandered lines in two directions.

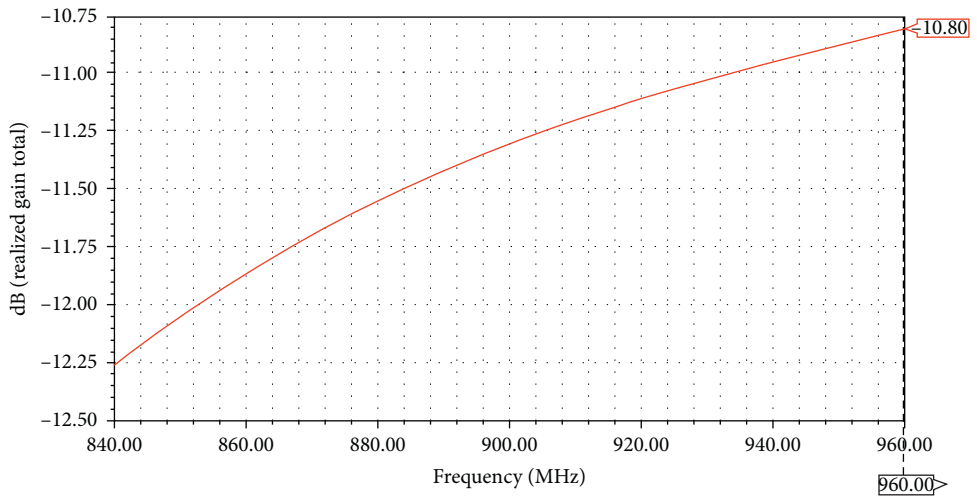

Figure 15: Simulated realized gain of the epidermal double-loop tag with meandered lines in two directions.

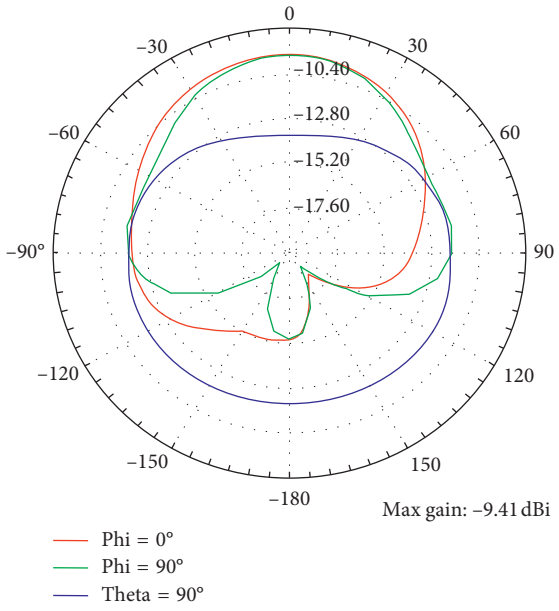

Figure 16: Radiation pattern (total gain) of the epidermal tag with meandered lines in two directions.

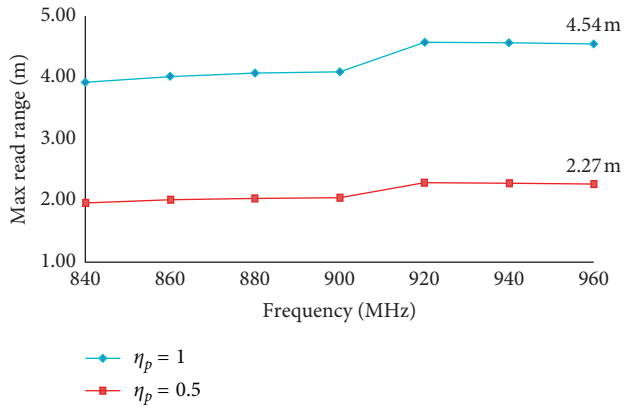

Figure 17: Simulated read range of the epidermal RFID double-loop tag with meandered lines in two directions for readers with circular (red line) and linear (blue line) polarizations.

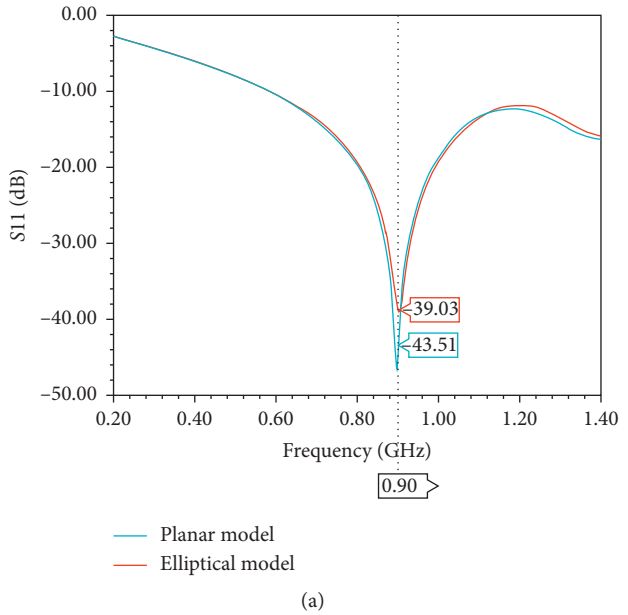

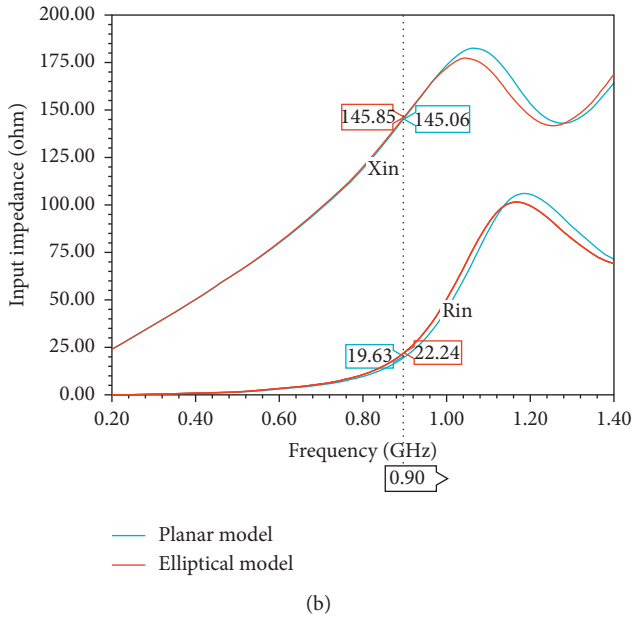

Figure 18: Simulated $S11$ (a) and antenna input impedance (b) of the second tag placed on layered elliptical and planar models.

tissues absorb some of the electromagnetic radiations. Therefore, accounting these losses in the human tissues, the total gain of the epidermal tag reaches −9.41 dBi in the (xy) plane at the resonance frequency of 960 MHz.

In Figure 17, the estimated reading range of the second epidermal tag is plotted versus the frequency, when the tag is placed directly on the reference model of human body. The maximum reading distance is almost 2.27 m in the case of the reader with circular polarization ($\eta p = 0.5$) and above 4.5 m in the case of the reader with linear polarization ($\eta p = 1$).

3.6. The Bending Effect on the Epidermal Tag with Meandered Lines in the Two Directions Design. Figure 18(a) shows simulated $S11$ of our second antenna by supposing, as above, the two reference models of the human torso: the planar and the elliptical model. $S11$, around the resonant frequency 900 MHz, of the second proposed antenna-bending format (−39 dB) is less than the one of the planar model (−43 dB). Figure 18(b) presents the input impedance of the second proposed antenna placed on the planar and elliptical model, and the elliptical model will slightly affect the impedance matching of the second proposed antenna which can be clearly described in this figure, showing a slightly change in the input resistance value at around 900 MHz, while its input reactance remains unchanged.

To confirm our results obtained by the HFSS solver, we proceeded by designing the same antenna in the CST

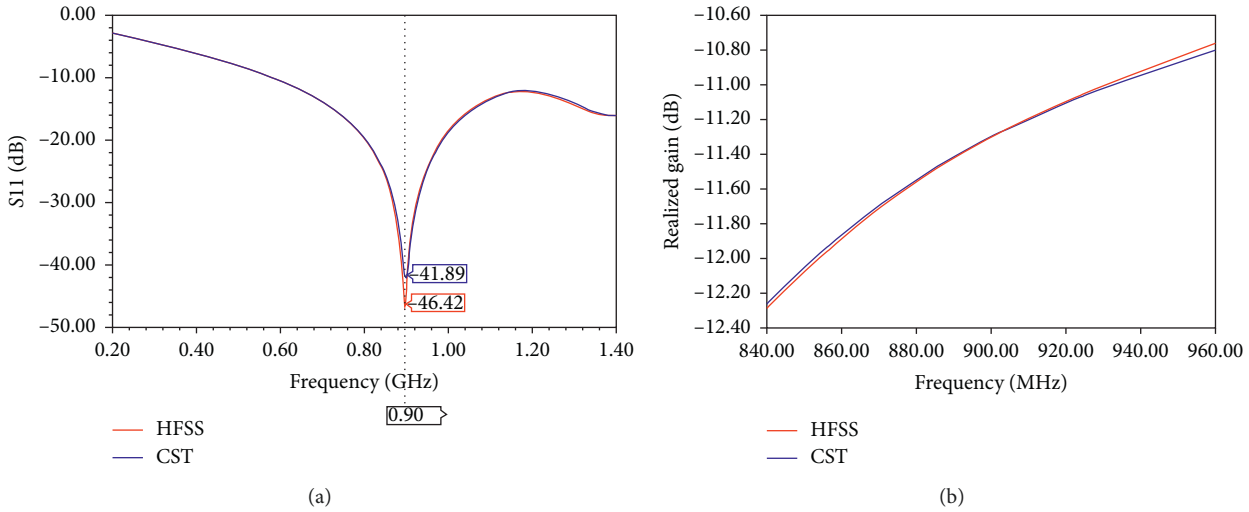

Figure 19: Comparison of S11 (a) and realized gain (b) results of the second antenna performed with the Ansoft HFSS and CST software.

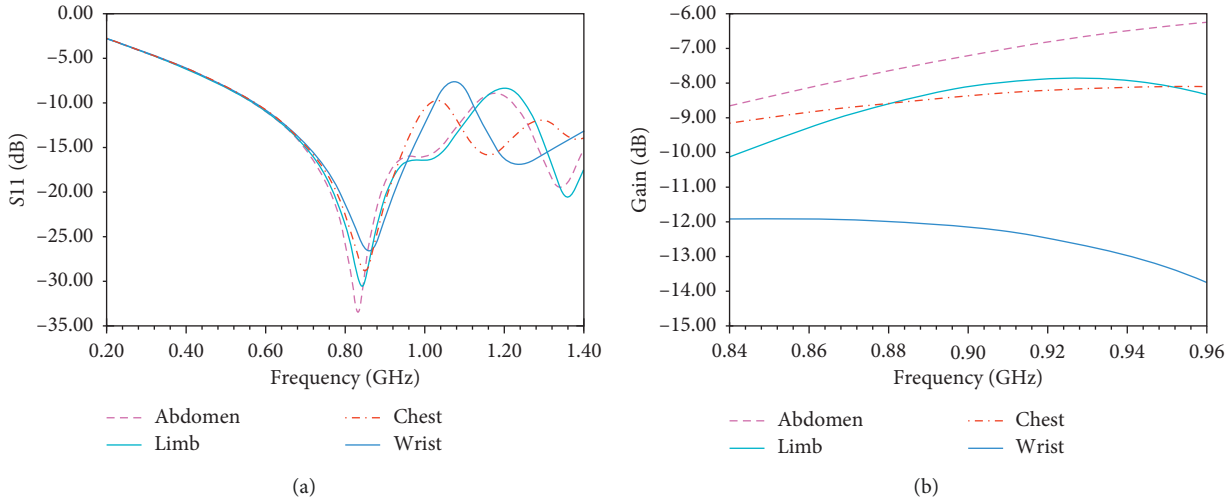

Figure 20: Simulated S11 (a) and gain (b) of the second epidermal proposed tag placed onto four reference layers models of some body parts.

simulator and performing the simulation of antenna properties. Figures 19(a) and 19(b) show a comparison between results of these two solvers. Similarly, S11 and realized gain values versus the frequency are obtained for both solvers. This indicates that using either HFSS or CST solvers converge to similar matching features and radiation performance.

3.7. Simulated Performances of the Second Proposed Antenna versus Human Body Parts. We have tested the matching characteristics and the gain of the second antenna by supposing, as above, different parts of the human body (limb, abdomen, chest, and wrist). Figure 20(a) shows a decrease of the simulated S11 of the second antenna around the resonance frequency, when it is placed in the limb and abdomen. This behavior is reflected in the total gain depicted in Figure 20(b) as a function of the frequency, where a difference is noticed between the human parts, the wrist, abdomen, chest, and limb. As stated above, this can be related to the larger fat tissue thickness of the abdomen, limb, and chest compared to the one of the wrist. Therefore, better total gains are obtained in the case of the abdomen and limb region.

4. Conclusion

The two proposed antennas configurations seem to be attractive to achieve miniaturized size and effective conjugate impedance to the microchip. Our simulations have demonstrated that the double-loop with meandered lines of epidermal UHF RFID tags insulated from the human skin by a flexible bio-silicone layer, provide a good realized gain. The wide bandwidths of the two antennas are enough to cover the worldwide UHF band. In addition, these two designed tags can be activated from a distance of almost 2.5 m up to 5 m depending on the position between the reader and the tag. We have verified and confirmed simulated features of

our designed tags obtained by the HFSS solver by using the CST simulator, especially in the case when the tag is bound to a rectangular anatomical human body shape. We have shown that these two particular structures are not much influenced by the detuning and absorbing effects on the human body.

Data Availability

We used in our work theoretical simulations with simulators; the data used to support the findings of this study are included within the article.

Conflicts of Interest

The authors declare that they have no conflicts of interest.

Acknowledgments

This work was supported by the Computer and Telecommunications Research Laboratory (LRIT), Associated Unit to CNRST (URAC29), Rabat IT Center, Faculty of Science, Mohammed V University, Rabat, and LaGeS, EHTP, Morocco.

References

[1] K. Finkenzeller, *RFID Handbook*, Wiley, Hoboken, NJ, USA, 3rd Edition, 2010.

[2] D. Dobkin, *The RF in RFID*, Elsevier, Burlington, MA, USA, 2007.

[3] G. Marrocco, "RFID antennas for the UHF remote monitoring of human subjects," *IEEE Transactions on Antennas and Propagation*, vol. 55, no. 6, pp. 1862–1870, 2007.

[4] J. Kim, A. Banks, H. Cheng et al., "Epidermal electronics with advanced capabilities in near-field communication," *Small*, vol. 11, no. 8, pp. 906–912, 2015.

[5] C. Occhiuzzi, S. Cippitelli, and G. Marrocco, "Modeling, design and experimentation of wearable RFID sensor tag," *IEEE Transactions on Antennas and Propagation*, vol. 58, no. 8, pp. 2490–2498, 2010.

[6] S. Manzari, C. Occhiuzzi, and G. Marrocco, "Feasibility of body-centric systems using passive textile RFID tags," *IEEE Antennas and Propagation Magazine*, vol. 54, no. 4, pp. 49–62, 2012.

[7] G.-L. Huang, C.-Y.-D. Sim, S.-Y. Liang, W.-S. Liao, and T. Yuan, "Low-profile flexible UHF RFID tag design for wristbands applications," *International Journal of Antennas and Propagation*, vol. 2018, p. 13, 2018.

[8] S. Amendola, S. Milici, and G. Marrocco, "Performance of epidermal RFID dual-loop tag and on-skin retuning," *IEEE Transactions on Antennas and Propagation*, vol. 63, no. 8, pp. 3672–3680, 2015.

[9] S. Amendola, G. Bovesecchi, A. Palombi, P. Coppa, and G. Marrocco, "Design, calibration and experimentation of an epidermal RFID sensor for remote temperature monitoring," *IEEE Sensors Journal*, vol. 16, no. 19, pp. 7250–7257, 2016.

[10] G. Marrocco, "The art of UHF RFID antenna design: impedance-matching and size-reduction techniques," *IEEE Antennas and Propagation Magazine*, vol. 50, no. 1, pp. 66–79, 2008.

[11] ANSYS HFSS 17.1, "EM simulation software," 2016, https://www.ansys.com/products.

[12] CST STUDIO SUITE 2016, "EM simulation software," 2016, https://www.cst.com/products.

[13] http://niremf.ifac.cnr.it/tissprop/.

[14] P. V. Nikitin, K. V. S. Rao, S. F. Lam, V. Pillai, R. Martinez, and H. Heinrich, "Power reflection coefficient analysis for complex impedances in RFID tag design," *IEEE Transactions on Microwave Theory and Techniques*, vol. 53, no. 9, pp. 2715–2721, 2005.

[15] L. Yang, A. Rida, and M. M. Tentzeris, "Design and development of radio frequency identification (RFID) and RFID-enabled sensors on flexible low cost substrates," *Synthesis Lectures on RF/Microwaves*, vol. 1, no. 1, pp. 1–89, 2009.

[16] C. Gabriel, S. Gabriel, and E. Corthout, "The dielectric properties of biological tissues: I. Literature survey," *Physics in Medicine and Biology*, vol. 41, no. 11, pp. 2231–2249, 1996.